

# Recent Research and Development in the Processing, Microstructure, and Properties of Titanium and Its Alloy

Mitsuo Niinomi<sup>1,2,\*</sup>, Takayuki Narushima<sup>3</sup> and Takayoshi Nakano<sup>2,4</sup>

<sup>1</sup>Institute for Materials Research, Tohoku University, Sendai 989-8577, Japan

<sup>2</sup>Division of Materials and Manufacturing Science, Graduate School of Engineering, Osaka University, Suita 565-0871, Japan

<sup>3</sup>Department of Materials Processing, Graduate School of Engineering, Tohoku University, Sendai 980-8579, Japan

<sup>4</sup>Anisotropic Design & Additive Manufacturing Research Center, Osaka University, Suita 565-0871, Japan

The special issue on recent research and development in the processing, microstructure, and properties of titanium and its alloy contains four review articles on metal additive manufacturing (AM) focusing on the processing, microstructural and/or crystallographic control, and biomedical applications of titanium and its alloys, and seventeen regular articles on metal AM, refining, microstructural evolution, and mechanical and fatigue properties related to the microstructure, and biomedical applications of titanium and its alloys, which have been published in Materials Transactions in 2023. This study briefly addresses this issue. [[doi:10.2320/matertrans.MT-M2024082](https://doi.org/10.2320/matertrans.MT-M2024082)]

(Received August 15, 2024; Accepted September 7, 2024; Published November 25, 2024)

**Keywords:** titanium and its alloys, additive manufacturing (AM), phase transformation, microstructure, mechanical properties, titanium based intermetallics, biomaterials, recycling

## 1. Introduction

For further development of titanium alloys, it is necessary to understand their physicochemical properties to increase their strength, improve their performance, lower their costs, and improve the sophistication of the process technology. Consequently, the World Conference on Titanium (formerly the Titanium International Conference) has been held every three or four years since 1968 as a forum for exchanging information on the latest science and technology of titanium alloys. Materials Transactions covered special issues on titanium in 2004 [1], 2009 [2], 2013 [3], 2017 [4], and 2019 [5].

Subsequently, the 15th Titanium World Conference on Titanium was held in Edinburgh, UK in June 2023. The Japan Institute of Titanium [6] was established in 2021 in Japan. A text book on titanium alloys, Fundamental and Applications of Titanium [7] was published. Based on this background, Materials Transactions published a special issue on Recent Research and Development in the Processing, Microstructure, and Properties of Titanium and Its Alloy in 2023 [8]. This special issue contains four review articles on metal AM focusing on processing, microstructural and/or crystallographic control, and biomedical applications of titanium and its alloys, and seventeen regular articles on metal AM, refining, microstructural evolution, and mechanical and fatigue properties related to microstructure, and biomedical applications of titanium and its alloys. This special issue was a joint publication of the Japan Institute of Metals and Materials and the Japan Institute of Light Metals.

This paper reviewed the latest Special Issue on Recent Research and Development in the Processing, Microstructure, and Properties of Titanium and Its Alloy published in No. 1, Vol. 64, 2023 of Materials Transactions [8].

## 2. Metal Additive Manufacturing (AM)

### 2.1 Effects of fabrication factors

Laser powder bed fusion (L-PBF) and electron beam powder fusion (EB-PBF) are typical powder bed fusion additive manufacturing (AM) for metallic materials [9].

Atmospheric gas selection in metal AM is important. EB-PBF is conducted in vacuum (generally, helium (He) gas under an order of  $10^{-1}$  Pa is used to suppress smoke), whereas L-PBF is typically performed in an argon (Ar) or a nitrogen ( $N_2$ ) atmosphere, depending on the metal, to remove spatter and fumes. The Ar and  $N_2$  gases exhibit similar heat conductivities and densities. He gas exhibits lower density and greater heat conductivity than Ar and  $N_2$  gases [10]. Therefore, the effect of atmospheric gas with a focus on the He gas atmosphere, which exhibits a high cooling rate, on the spattering, microstructure and mechanical properties of the fabricated products is interesting. The effect of atmospheric gas selection in metal AM on the spattering, microstructure and mechanical properties of the fabricated products, in particular, the Ti-6Al-4V product in L-PBF was reviewed by Amano *et al.* [11].

The spattering was suppressed considerably more in He gas atmosphere than in Ar gas atmosphere. This trend was similar even when the oxygen content in Ti-6Al-4V was increased, indicating that He gas atmosphere is advantageous for the recycling Ti-6Al-4V. The grain size of Ti-6Al-4V product was reduced and its mechanical properties (tensile strength, 0.2% proof stress, and elongation) were improved under He gas atmosphere. Therefore, in the future, the active use and control of gas-related factors are expected to expand the control range of the microstructure and mechanical/chemical properties of L-PBF-fabricated metal products.

Metal AM can be utilized in future manufacturing as a technology that has the potential to 'create' internal microstructures unachievable from other technologies, as well as produce three-dimensional shapes with high accuracy including surface accuracy.

\*Corresponding author, E-mail: Mitsuo.niinomi.b6@tohoku.ac.jp

Ishimoto and Nakano [12] have reviewed the microstructure that dictates the essential part of mechanical properties of the product, in addition to the shape properties, as well as the latest microstructural developments that are unique to the PBF of light metal materials with a focus on titanium alloys.

The most commonly produced light-metal AM materials are titanium and aluminum alloys. The commonly manufactured Ti alloy using metal AM is the ( $\alpha + \beta$ )-type Ti-6Al-4V alloy. From a microstructural perspective, the Ti-6Al-4V alloy undergoes a phase transformation from the bcc- $\beta$  phase to the hcp- $\alpha$  ( $\alpha'$ ) phase when cooled. Furthermore, for the Ti-6Al-4V alloy, structure size change and martensite ( $\alpha'$ ) phase formation as a function of the cooling rate, changes in structure/phase composition owing to repeated thermal history peculiar to AM non-uniformity in members etc. have been extensively investigated. The  $\beta$ -type titanium alloys such as Ti-15Mo-5Zr-3Al alloys basically do not undergo phase transformation to the  $\alpha$  phase during quenching. Therefore, unlike in the case of the Ti-6Al-4V alloy, the crystal orientation of the  $\beta$  phase in such alloys was maintained during solidification. However, in the case of an alloy containing a metastable phase, phase transformation may occur owing to its thermal history during fabrication and generation of residual stress.

One of the greatest characteristics of AM of metals, especially PBF, is the formation of a strong crystallographic texture on metallic materials. The crystallographic texture causes anisotropy of mechanical properties such as Young's modulus, yield stress, and wear resistance. For example, in single crystals of some  $\beta$ -type titanium alloys, especially alloys with a small average valence electron number per atom  $e/a$  ( $e$ : total number of valence electrons,  $a$ : total number of atoms), which is close to 4, the Young's modulus drops to approximately 40 GPa along the  $\langle 100 \rangle$  direction, owing to anisotropy [13]. This is expected to suppress stress shielding and could be relevant when considering the material for application as a bone implant. To obtain a single crystal, for instance, the floating zone method produces single crystals by moving the solid-liquid interface at a low speed of several mm/h ( $10^{-4}$ – $10^{-3}$  mm/s). In L-PBF, the solid-liquid interface migrates at high speed, owing to the travel speed of heat source ( $\sim 10^3$  mm/s). However, the extremely large temperature gradient ( $\sim 10^3$  K/mm) ensures flat interface migration, and strong crystallographic texture can be obtained through epitaxial growth by stabilizing the crystal orientation. Crystallographic texture formation depends on the scan strategy in L-PBF as shown in Fig. 1 [12], as well as on the molten pool shape; a single crystal-like lamellar structure is obtained in the  $\beta$ -type Ti-15Mo-5Zr-3Al alloy. A polycrystalline structure with a relatively isotropic crystal orientation can easily be obtained by laser scanning under the conditions in which two-dimensional solid-liquid interface migration in the cross-section of the molten pool is not established. Specifically, a polycrystalline structure is achieved by shortening the tail of the molten pool and maintaining a large inclination at the bottom of the molten pool along the scanning direction. An example is shown for the  $\beta$ -type Ti-15Mo-5Zr-3Al alloy.

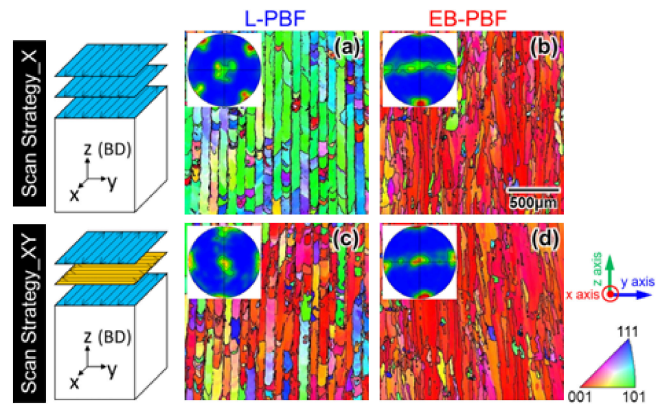


Fig. 1 Differences in the crystallographic textures of Ti-15Mo-5Zr-3Al alloy fabricated by L-PBF and EB-PBF, and as a function of the scan strategy of heat sources.  $yz$  cross section was observed and the crystallographic orientation was projected in the  $z$  direction. In (a) and (c) for L-PBF, the crystallographic textures of  $\{011\}z(100)x$  and  $\{001\}z(100)x$  are formed depending on the scan strategy. However, in (b) and (d) for EB-PBF, the texture of  $\{001\}z(100)x$  is obtained in both scan strategies X and XY.

Metal AM is being recognized as a technology for controlling the microstructure of metals rather than its shape, or as a methodology for simultaneously controlling the shape as well as microstructure.

Parts with satisfactory quality and without defects can be manufactured using PBF-AM only when the powder-raking process conditions and beam irradiation parameters are appropriate [14]. Therefore, it is important to understand the effects of powder properties and raking process conditions on the properties of powder beds for quality assurance of PBF-manufactured parts.

Okugawa *et al.* [15] have reviewed the influences of the powder raking process conditions on the densities and homogeneity of powder bed by computer simulation using the DEM and an experiment of powder bed formation using a blade-type spreader for Ti-6Al-4V alloy powder by way of example. The results were analyzed with a special focus on the effects of the relative size of the powder particles with respect to the gap between the blade and the build platform. It has been shown that the gap should be larger than the upper bound of the distribution of powder particles diameter to obtain a high-density powder bed. The DEM simulation indicated that the blade could sweep powder particles that were not in direct contact with the blade when the powder particles are in a close-packed tetragonal configuration. This is because powder particles smaller than half of the gap are suitable for PBF.

The wettability between a liquid and its own solid, which is an important physicochemical property of materials under metal AM is an interfacial property related to the material bonding and is one of the control factors in powder bed fusion. Although good wettability guarantees bonding between layers owing to the easy spreading of the liquid on the solid, poor wettability causes defects owing to a lack of bonding [16]. Knowledge of wettability is essential for a deep understanding of such interfacial phenomena and simulation with high accuracy. However, data on the wettability of a liquid and its solid for metal systems are limited.

Nakamoto *et al.* [17] measured two interfacial properties, the contact angle and interfacial tension, between a liquid Ti-6Al-4V alloy and its solid using the surface morphology of a sample built by electron-beam additive manufacturing with powder bed fusion. They found that the contact angle between the liquid and solid phases of the Ti-6Al-4V alloy could be accurately measured using the 3D morphology of the side surface of a built sample, and the contact angle and interfacial tension between the liquid and solid phases of the Ti-6Al-4V alloy were  $12^\circ$  and 376 mN/m, respectively.

The complex thermal history of AM is accompanied by rapid and local thermal shrinkage; therefore, residual stress is likely to occur in fabricated parts. In addition, when dealing with a material that exhibits an unstable phase, such as  $\beta$ -type titanium alloys, there is a concern that undesired phase changes may occur, depending on the thermal history. Residual stress causes the deformation of the outer shape of the part during or after the manufacturing process. Concurrently, the residual stress near the surface causes cracks, which reduces the mechanical reliability of the final part [18]. Changes in the crystalline phase caused by the stabilization of a metastable phase by residual stress can unintentionally affect the performance and reliability of the final part because of changes in the mechanical properties of the material. Therefore, it is essential to systematically relate various process conditions to the residual stress and phase stability of the resulting product and to optimize the process conditions to realize the required functionality of the final parts.

Takase [19] has reviewed a method that combines the X-ray diffraction (XRD) method and numerical simulation of the thermal history during the manufacturing process with two examples of titanium alloys, ( $\alpha + \beta$ )-type Ti-6Al-4V and  $\beta$ -type Ti-15Mo-5Zr-3Al alloys, fabricated by L-PBF and EB-PBF.

In the PBF technique, the thermal histories during and after solidification are exceptionally complicated. In addition, the final constituent phases of Ti-based alloy changes depending on the alloy composition and thermal history. Recently, the control of crystal texture (crystal orientation) using the PBF technique has garnered attention. The process conditions that simultaneously reduce residual stress and the desired crystal phase and texture do not always match. When forming an unstable phase, such as in the  $\beta$ -type Ti-15Mo-5Zr-3Al alloy, it is necessary to consider the effect of residual stress on phase stability. However, when forming a phase with solid phase transformation, such as the ( $\alpha + \beta$ )-type Ti-6Al-4V alloy, it is necessary to optimize the process conditions after evaluating the cooling rate immediately after solidification, which affects the residual stress, as well as the cooling rate near the  $\beta$  transus temperature, which simultaneously affects the crystalline phase. Furthermore, when a laser is used as the heat source, the cooling rate has a larger effect on the residual stress and phase stability compared to an electron heat source. Meanwhile, when using an electron beam, annealing by preheating primarily affects the phase stability. Therefore, it is necessary to select an AM method that consider the different thermal histories corresponding to each heat source. It is essential to systematically and quantitatively evaluate and understand the relationships among the heat

source, process conditions, residual stress, and crystallographic properties to realize parts with excellent mechanical properties that satisfy all structural requirements. An analysis method that combines XRD and numerical temperature simulation is effective.

## 2.2 Applications to special titanium-based alloys: Composite, high temperature alloy, intermetallic compound, biomaterial, and high entropy alloy

Ti-6Al-6Nb-4Zr alloy was developed for high temperature applications at a temperature greater than  $600^\circ\text{C}$ . The microstructural evolution and high temperature mechanical properties of the forged Ti-6Al-4Nb-4Zr alloy were already investigated [20]. However, microstructures and high temperature mechanical properties (creep properties) including room temperature mechanical properties (compressive properties) of Ti-4Al-4Nb-4Zr alloy fabricated by AM remain unclear.

Kuroda *et al.* [21] investigated the microstructural evolution and related high-temperature mechanical properties of Ti-6Al-4Nb-4Zr alloys fabricated using PBF-AM. In this case, L-PBF was utilized because it was expected to result in a drastic change in the microstructure owing to the faster cooling rate compared with that in EB-PBF.

Under rapid cooling, the martensitic structure formed a scale-like pattern, with a size of  $100\ \mu\text{m}$ , which is consistent with the laser scanning pattern. However, under slow cooling conditions, the  $\alpha/\beta$  lamellar structure formed in  $\beta$  grains with a grain size of  $300\ \mu\text{m}$  instead of scale-like pattern. The martensitic structure significantly changed to an Widmanstätten structure during heat treatment. An equiaxed  $\alpha$  phase is also formed at the interface of the scale-like patterns. However, the  $\alpha/\beta$  lamellar structure did not exhibit a change in response to heat treatment. The compressive strength of the L-PBF samples was governed by the martensite and grain sizes, both of which depend on the cooling rate. The dominant creep deformation mechanism at  $600^\circ\text{C}$  and under a loading stress of 137 MPa formed grain boundary sliding. The creep life depends on the grain size. HIP treatment improves creep life because it eliminates pores introduced by the L-PBF process.

The hardness and tribological properties of titanium and its alloys are poor [22]. Therefore, the fabrication of ceramic-particle-reinforced titanium matrix composites (TMCs) is considered an effective way to achieve desirable properties. Among the various ceramics, graphene is the most promising candidate for the fabrication of high-performance TMCs. Graphene/metal matrix composites exhibit significantly improved mechanical properties such as tensile strength and wear resistance. Spark plasma sintering (SPS) is a popular densification process for TMCs [23] based on the simultaneous application of high pressure and high temperature. It has the advantages of low sintering temperatures, reduced sintering time, negligible grain growth, and energy conservation [24]. Owing to rapid solidification ( $\sim 10^3\text{--}10^8\ \text{K}\cdot\text{s}^{-1}$ ) induced by high-energy laser irradiation, L-PBF-processed composites exhibit ultrafine microstructures and promising properties [25]. However, the microstructure and mechanical performance of additive-manufactured graphene-reinforced TMCs have not been studied extensively.

The densification process plays a critical role in determining the microstructures of TMCs, for example, the dispersion state of fillers, interfacial bonding, and texture information of the matrix, thereby influencing their properties.

Dong *et al.* [26] have employed two typical densification processes, L-PBF and SPS, to fabricate graphene oxide (GO)-reinforced Ti-6Al-4V alloy composites. The structural evolution mechanism of GO during high-temperature densification is elucidated. The mechanical performance of the two TMCs are compared and discussed based on microstructural observations. Flexible GO sheets can be homogeneously decorated on Ti-6Al-4V alloy powders via electrostatic self-assembly without significantly changing the particle size or sphericity. Under high-energy laser irradiation, the GO sheets are completely dissolved into the matrix. The L-PBF-produced composite was composed of fine  $\alpha'$  martensite structures owing to rapid solidification and solute carbon atoms. However, GO reacted with the Ti matrix and was completely transformed into submicron TiC particles during SPS; the composite consisted of the  $\alpha + \beta$  phases with randomly dispersed TiC. Moreover, the L-PBF-produced composite exhibited a higher hardness (481 HV) than the SPS-produced composite (367 HV), which was attributed to its fine microstructures and high residual stresses. The present study offers a deeper understanding of the structural evolution of GO during high-temperature densification, and provides new insights into the fabrication of high-performance TMCs with tailored microstructures.

In the fabrication of titanium-based intermetallic TiAl alloys ( $\gamma$ -TiAl), EB-PBF has received considerable attention because the residual stress in the products is less than that in products fabricated using L-PBF [27].

$\gamma$ -TiAl and Ti-48Al-2Cr-2Nb (at%, hereafter 4822) alloys, which have already been practically applied, can be successfully fabricated using an EB-PBF, and a unique layered microstructure composed of a duplex structure (equiaxed  $\gamma + \alpha_2/\gamma$  lamellar grains) and near  $\gamma$  structure regions were obtained [28]. The near  $\gamma$  structure region is referred to as the  $\gamma$  band. The formation of the layered microstructure is closely related to the repeated melting of the raw powders and the temperature distribution in the molten pool formed at each melting point. Therefore, the layered microstructure could be oriented in any direction by changing the building direction. In particular, an alloy with a layered micro structure oriented at  $45^\circ$  in the loading direction exhibits excellent high-temperature strength and fatigue strength [29]. However, the relationship between the process conditions and morphology of the layered microstructure has not been clarified.

Cho *et al.* [30] examined the effect of input energy density (ED) on the morphology of the layered microstructure of 4822 alloys, focusing on the width of the  $\gamma$  band and the volume fractions of the  $\gamma$  and  $\alpha_2$  lamellar grains in the duplex region has been examined. They also examined the change in the strength and ductility of the alloys at room temperature with the change in the microstructure according to the change in ED. A unique layered microstructure consisting of an equiaxed  $\gamma$ -grain layer ( $\gamma$ -band) and a duplex region can be formed by EB-PBF with an ED in the range of 13 to 31 J/mm<sup>3</sup>. However, the width of the  $\gamma$ -band and the volume

fraction of the  $\gamma$ -phase in the duplex region decrease with increasing ED. In contrast, the number of  $\alpha_2/\gamma$  lamellar grain in the duplex region increases with increasing ED. These morphological changes in the layered microstructure were attributed to the variation of temperature distribution of the molten pool caused by the increasing ED. The strength of the alloys can be improved by decreasing the width of the  $\gamma$ -band and increasing of the number of  $\alpha_2/\gamma$  lamellar grain in the duplex region. However, the width of the  $\gamma$ -band and the fraction of equiaxed  $\gamma$ -grains in the duplex region should be increased to enhance the ductility of the alloys. The strength-ductility balance of the alloy fabricated using EB-PBF was better than that of HIP-treated cast alloys.

Gokan *et al.* [31] investigated the effect of the energy density with different beam currents, beam speeds, and hatching spaces as process parameters on the microstructure and high-temperature tensile and creep properties of 4822 fabricated by EB-PBF.

Porosity and surface roughness decreased with increasing energy density. In addition, the fraction of lamellar structures tended to increase with increasing the energy density. However, an increase in lamellar structure does not necessarily lead to any improvement in tensile or creep strength at 750°C. A constant energy density of 15 J/mm<sup>3</sup> shows better tensile and creep properties than the standard parameters. Therefore, it is important to optimize the parameters according to the required properties of the parts.

Titanium and its alloys are widely used in dentistry and orthopedics as metallic medical materials, to replace failed hard tissue (bone tissue). Metal AM can impart structural anisotropy and complex structures to the surfaces and interiors of metallic materials. AM is widely regarded as a powerful next-generation technology for realizing anisotropic high-performance materials that imitate bone function. In particular, the key to recovering lost bone function is the induction of the expression of functionality required in three dimensions, based on the anisotropic structure of the original bone tissue.

Matsugaki *et al.* [32] have reviewed the current developments in controlling hard-tissue compatibility by three-dimensional modeling of titanium alloys and outlined the latest findings of bone medical device research for guiding anisotropic bone microstructure.

First, the current development in hard-tissue compatibility research using metal AM is described.

The Young's moduli of metallic implants must be similar to that of bone from the view-point of mechanical biocompatibility, leading to the creation of implants that can suppress stress shielding [33]. The Young's moduli of titanium alloys are the lowest among the typical metallic biomaterials. Metal AM can control the crystallographic texture, enabling physical property control based on the orientation dependence of mechanical properties such as Young's modulus [34]. Metal AM can produce porous structures with a lower Young's modulus and appropriate porosity and pore size including changes in body fluid inflow, cell invasion, proliferation, and differentiation ability [35]. Controlling complex internal shapes using this method is effective in inducing direct coupling of the device with bone: osseointegration properties. The shape of the material surface

significantly affects the manifestation of these characteristics. It has been reported that control of the structural surface shape using a scanning electron beam or a laser beam induces osteoblast proliferation [36] collagen matrix secretion [37] and stem cell differentiation [38], all of which depend on surface roughness. Furthermore, recently, it has been reported that the shaping direction and process parameters also control the proliferation and gene expression of stem cells. Cellular responses, including cell adhesion through protein adsorption and transcription factor expression in the cell nucleus, have been proposed as cell-guiding cues for structural control of metal materials. For functional bone reconstruction, it is essential to effectively use these interactions between living organisms and materials and to connect the bone-device interface with a functionally fused bone. Bone exerts its necessary functionality in three dimensions by hierarchically constructing an anisotropic tissue. The formation of anisotropic tissue is indispensable for the soundness of the bone, which must start from the interactions between the bone medical device and the living tissue. Bone medical devices that can induce bone functionalization based on an anisotropic microstructure peculiar to living bone using a metal AM technology have been developed [39].

Subsequently, they outlined the latest findings of bone medical device research for guiding anisotropic bone microstructure.

The collagen/apatite crystal *c*-axis shows an anisotropic arrangement for the maximum principal stress vector direction; thus, showing high strength in the orientation direction [40]. Living bone exhibits high-strength in the required direction owing to the crystal aggregates. It is difficult to spontaneously reconstruct bone orientation in diseased and regenerated bones that have lost their appropriate anisotropy; even if bone density has substantially recovered. To regain bone function, the development of a medical device that artificially induces the repair of lost bone orientation is indispensable. The use of artificial materials to express the anisotropy function at the interface between living tissues is the key to achieving this goal. To establish anisotropic bone reconstruction, it is important to control the unidirectional arrangement of osteoblasts responsible for bone regeneration. Metal AM manufacturing, which can help control surface structures at the submillimeter scale, enables fluid inflow guide cellular components on the device surface [41]. For example, arrangement of mesenchymal stem cells along a unidirectional pattern formed by a laser beam with a groove width of 250  $\mu\text{m}$  was reported [41]. Surface structural control using metal AM enables functional bone reconstruction from the initial regeneration stage even without loading.

When bone formation around the device is achieved, the continuous transmission of the maximum principal stress vector to the bone is essential for bone health. Dental implants, artificial hip joint stems [66] and spinal fixation devices (cages) made of Ti-6Al-4V alloys with a bone-orientation-guided design, such as oriented grooves and oriented porous bodies named honeycomb tree structure (HTS) created by metal AM have been approved by regulatory affairs and launched on the market.

Recently, the three-dimensional organs and organoid developed using living cells as raw materials and bioprinting

technology has advanced and is expected to be applied in regenerative medicine.

Matsugaki *et al.* [42] also created an anisotropic mini-bone organ similar to bone by controlling single-cell drawing and the molecular arrangement of protein using inkjet bioprinting.

Titanium contained high entropy alloy (HEA), the Ti-Zr-Nb-Ta alloy for biomedical applications, was first developed by Nakano's research group at Osaka University, Japan [43]. Subsequently, the research group developed the Ti-Zr-Hf-Y-La system [44], Ti-Zr-Hf-(Co)-Cr-Mo system [45] and Ti-Zr-Hf-Nb-Ta-Mo system BioHEA [46].

BioHEAs manufactured using a casting method exhibit a strong tendency toward phase separation based on elemental segregation. Therefore, a uniform solid solution was not obtained for the cast BioHEAs. L-PBF has a fast solidification rate and can be considered an effective method for forming a uniform solid solution for BioHEAs.

Ozasa *et al.* [47] have reviewed the research and development of titanium-containing BioHEAs fabricated using a laser powder bed fusion.

A non-equiatomic  $(\text{TiZr})_{1.4}(\text{NbTaMo})_{0.6}$  alloy, which satisfies the solid solution formation conditions of the parameter method, was developed based on the equiatomic TiZrNbTaMo alloy [48]. The non-equiatomic  $(\text{TiZr})_{1.4}(\text{NbTaMo})_{0.6}$  alloy exhibits improved ductility while maintaining the same yield stress as the equiatomic TiZrNbTaMo alloy under cast conditions. Dendrite structures causing phase separation and elemental segregation were observed in the  $(\text{TiZr})_{1.4}(\text{NbTaMo})_{0.6}$  alloy under cast conditions. However, the  $(\text{TiZr})_{1.4}(\text{NbTaMo})_{0.6}$  alloy fabricated by L-PBF exhibited a uniform elemental distribution, improved mechanical properties, and cell viability compared with those of the cast alloy as shown in Fig. 2 [47]. For example, it has a higher 0.2% proof stress than that of existing metallic biomaterials, such as commercially pure (CP) Ti, SUS316L stainless steel, and cast

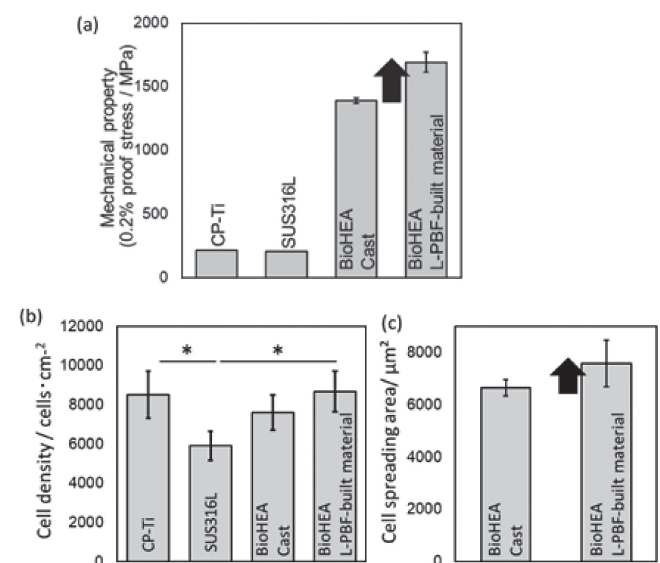


Fig. 2 (a) and (b) Mechanical properties and osteoblast cell density in  $(\text{TiZr})_{1.4}(\text{NbTaMo})_{0.6}$  alloys (BioHEA) fabricated using L-PBF and casting methods, and commercially pure Ti (CP-Ti) and SUS 316L stainless steel, (c) osteoblast cell spreading in  $(\text{TiZr})_{1.4}(\text{NbTaMo})_{0.6}$  alloys (BioHEA) fabricated using L-PBF and casting methods. \*:  $P < 0.05$ .

(TiZr)<sub>1.4</sub>(NbTaMo)<sub>0.6</sub> alloy [49] owing to grain refinement strengthening, solid solution hardening, and cell structure obtained through L-PBF, which results in ultra-rapid solidification rate [50].

### 3. Phase Transformation

The oxygen addition in a Ti alloy, in general, suppresses athermal  $\omega$  phase ( $\omega_a$ ) formation. However, the effect of the oxygen addition on the isothermal  $\omega$  phase ( $\omega_i$ ) formation is under investigation. Froes *et al.* [51] examined the formation kinetics of the  $\omega_i$  phase in the  $\beta$  matrix in the Ti-11.5Mo-6Zr-4.5Sn alloy (Beta III) with different oxygen levels of 0.17 and 0.28 mass%. They showed that increasing the oxygen content accelerated the kinetics of  $\omega_i$  phase formation and retarded those of  $\omega_a$  phase formation. Niinomi *et al.* [52] investigated the stability of  $\omega_i$  phase precipitates using two-step aging in a Ti-29Nb-13Ta-4.6Zr alloy. The stability of  $\omega_i$  particles formed by the first step aging at 300°C was increased as oxygen content increased from 0.1 to 0.4 mass% in the second step aging at 450°C. The partitioning of oxygen to the  $\omega_i$  particles was confirmed, and the high concentration of oxygen in the  $\omega_i$  particles stabilized the  $\omega_i$  phase. Chou and Marquis [53] investigated the influence of oxygen on the  $\omega_i$  precipitation during aging in the Ti-20 at%Nb alloy with up to approximately 5 at%O. They also have reported that oxygen increases the  $\omega_i$  phase stability. Therefore, there are discrepancies in the role of oxygen addition on the  $\omega_i$  phase formation. Acceleration or suppression of the  $\omega_i$  phase may vary depending on the  $\beta$ -stabilizers concentration as well as on the oxygen concentration.

Kobayashi *et al.* [54] have studied the effect of oxygen addition on the microstructure formation during cooling from the  $\beta$ -phase in the Ti-(13–20) at%Nb-(0–3) at%O alloy, of which ingots were arc-melted, homogenized, and then hot-rolled into 1.5 mm thick sheets. A disk specimen of 3 mm diameter was machined from 1.5 mm thick sheets and heated up to  $\beta$ -phase field at 1000°C in the differential thermal analysis apparatus. The specimens were cooled to room temperature at a rate of 20°C/min. The differential thermal analysis has proved that  $\beta \rightarrow \alpha$  transformation is accelerated by the oxygen addition in Ti-(13–15) at%Nb alloys, while the oxygen addition promoted  $\beta \rightarrow \omega_i$  transformation in Ti-(16–20) at%Nb alloys. The promoting effect on  $\beta \rightarrow \omega_i$  transformation increases up to 1.5% oxygen, but the effect weakens by adding more than 1.5 at% oxygen in Ti-(18–20) at%Nb alloys. The addition of oxygen over 3.0 at%O suppresses the  $\beta \rightarrow \omega_i$  transformation in Ti-20 at%Nb alloy.

The metastable phase characteristics of titanium alloys can be used to improve their functional properties such as Young's modulus, shape memory effect, and superelasticity. In particular, the hcp- $\alpha'$  and orthorhombic- $\alpha''$  martensite structures in titanium alloys provide suitable functional properties, such as a low Young's modulus and high damping. In the Ti-Nb binary alloys, Ti-(15–20) mass%Nb alloys corresponds to this compositional range.

Among metastable titanium alloys, several studies have focused on  $\beta$ -type Ti-Nb alloys with compositions in the Ti-(35–42) mass%Nb (22–27 at%Nb) range, which exhibit

shape memory and superelastic functions owing to the deformation-induced  $\alpha''$  martensite in the metastable  $\beta$ -phase [55]. The correlations between the material properties and stress and temperature applications remain unclear, although several studies have examined the metallographic characteristics [56] or material properties of ( $\alpha + \beta$ )-type titanium alloys with the quenched martensite structure [57].

Mantani and Takemoto [58] have investigated structural changes in the metastable quenched martensite structure of Ti-(10–20)Nb alloys subjected to heating and tensile strain using differential scanning calorimetry (DSC) heating curves in the reduction state, X-ray diffraction (XRD) profiles under loading-unloading, and material properties, such as Young's modulus and internal friction upon heating. In the DSC heating curve of the 10%-cold-rolled Ti-15Nb alloy, an exothermic peak was observed; and for Ti-18Nb and Ti-20Nb alloys, the exothermic peak exhibits broadening. The underlying reason is the biphasic formation, ( $\alpha'$  and  $\alpha''$  martensites), resulting from specimen deformation. From the XRD measurements, it was found that the lattice tended to shrink upon stress application and recover upon unloading. Significant changes in Young's modulus and internal friction are observed in the  $\alpha''$  martensite structures of Ti-18Nb and Ti-20Nb alloys during initial heating up to 373 K (100°C). Material properties change owing to structural changes, such as lattice-constant changes, biphasic formation, and crystal orientation changes, resulting from heating or plastic deformation.

### 4. Microstructure and Mechanical Properties

The mechanical properties of titanium alloys are often not entirely understood because of its history of practical applications is considerably shorter than that of steel or aluminum. For example, many reports have indicated that the yield stress of pure titanium follows the Hall Petch relation [59]. Nevertheless, various Hall-Petch coefficients have been reported in the literature [60]. The reported Hall-Petch coefficients vary considerably owing to an experimental cause, that is, the small amount of data obtained under different stress conditions. Furthermore, uncertainties have been noted regarding the size effects, which are the effects of the sample dimensions on the mechanical properties. The size effects on mechanical properties (on 0.2% proof stress) of pure iron, aluminum alloys, copper alloys, and austenitic stainless steel SUS316L have been confirmed as relationship between 0.2% proof stress and  $t/d$  (where  $t$  is the sheet thickness and  $d$  is the average grain diameter) or  $D/d$  (where  $D$  is the wire diameter and  $d$  is the grain size) by Miyazaki *et al.* [61] and Fukumaru *et al.* [62]. However,  $t/d$  dependence of 0.2% proof stress in CP Ti JIS class 1 cold-rolled sheet remains unclear [63].

Takebe *et al.* [64] examined the yield phenomena during the tensile testing of pure titanium sheets of 0.2 mm and 0.4 mm in thickness focusing on the effects of grain size ( $d$ ), thickness ( $t$ ),  $t/d$  ratio and tensile direction and the Hall-Petch coefficient ( $k$ ). With decreasing grain size, the yielding behavior changed from continuous yielding to one accompanied by a decrease in the yield point. Upper and lower yield stresses and 0.2% proof stress follow the Hall-Petch

relationship, but coarse-grained specimens ( $d \geq 20 \mu\text{m}$ ) show larger scatter in 0.2% proof stress than those of the other grain size specimens. Consequently, the Hall-Petch coefficient ( $k$ ) and friction stress ( $\sigma_0$ ) derived from 0.2% proof stress are not accurate enough. The values of  $k$  and  $\sigma_0$  derived from various yield stresses and tensile directions are in the range of  $250\text{--}600 \text{MPa}\cdot\mu\text{m}^{0.5}$  and  $30\text{--}180 \text{MPa}$ , respectively. Therefore, the validity of stress for yield stress is a concern, and the combination of the lower yield stress in the fine grain range ( $d \leq 20 \mu\text{m}$ ) and 0.2% proof stress excluding work-hardening in the coarse grain range ( $d > 20 \mu\text{m}$ ) is suggested to obtain reliable values of  $k$  and  $\sigma_0$  resulting in values of  $370\text{--}460 \text{MPa}\cdot\mu\text{m}^{0.5}$  and  $651\text{--}40 \text{MPa}$ , respectively. Moreover,  $k$  decreases and  $\sigma_0$  increased with increasing angle of the tensile direction to the rolling direction, regardless of the thickness. The anisotropy of  $k$  is presumed to be affected by the grain boundary characteristics rather than the Schmid factor, and neither the rigidity nor the length of the Burgers vector is responsible. The anisotropy of  $\sigma_0$  was verified to be affected by Schmid factors. Furthermore, the  $t/d$  ratio hardly affects upper and lower yield stresses ( $t/d > 14$ ) nor 0.2% proof stress ( $1.5 \leq t/d \leq 14$ ).

The  $(\alpha + \beta)$ -type Ti-6Al-2Sn-4Zr-2Mo-Si (Ti-6242S) alloy was used to replace the Ti-6Al-4V alloy owing to its enhanced high temperature performance [65]. However, compared to other metals, such as steels, the work hardening properties of titanium alloys are relatively low. Increasing the work hardening (maintaining high strength and high ductility) improves the homogeneous deformation behavior, toughness, damage tolerance, and energy absorption ability of titanium alloys [66] and promotes their usage.

The mechanical properties of the  $\alpha'$  martensite alone are poor in titanium alloys such as Ti-6242S alloy. However, when the  $\alpha'$  martensite is coupled with  $\alpha$ -phase, that is,  $(\alpha + \alpha')$  microstructure exhibits improved strength and ductility properties [67].

Séchépée *et al.* [68] applied a new type of microstructural control based on a non-equilibrium phase, the  $\alpha'$  phase with an HCP structure to enhance the mechanical properties (strength and ductility) of Ti-6242S with the effects of equiaxed  $\alpha$  and bimodal structures, which are both  $(\alpha + \beta)$  structures.

As for tensile properties in relation to microstructural factors, the correlations for the equiaxed  $\alpha$  microstructure shows that strength can be easily controlled by grain size (Hall-Petch law) and that the  $\beta$ -phase controls work-hardening. The equiaxed microstructures were found to be especially ductile (high plastic elongation) with good work-hardening, whereas the strength was average compared with the bimodal  $(\alpha + \beta)$  and duplex  $(\alpha + \alpha')$  microstructures. However, a high strength (but with a low work-hardening rate) was exhibited in the case of the bimodal  $(\alpha + \beta)$  microstructure. The duplex  $(\alpha + \alpha')$  microstructure showed great control of the strength and work-hardening owing to the formation of  $\alpha'$  martensite. Moreover, the balance between strength and work-hardening in the duplex  $(\alpha + \alpha')$  microstructure is interesting because it achieves high work-hardening and good strength as shown in Fig. 3 [68]. Nonetheless, the ductility of the duplex microstructure was excellent. The machine learning model using the gradient

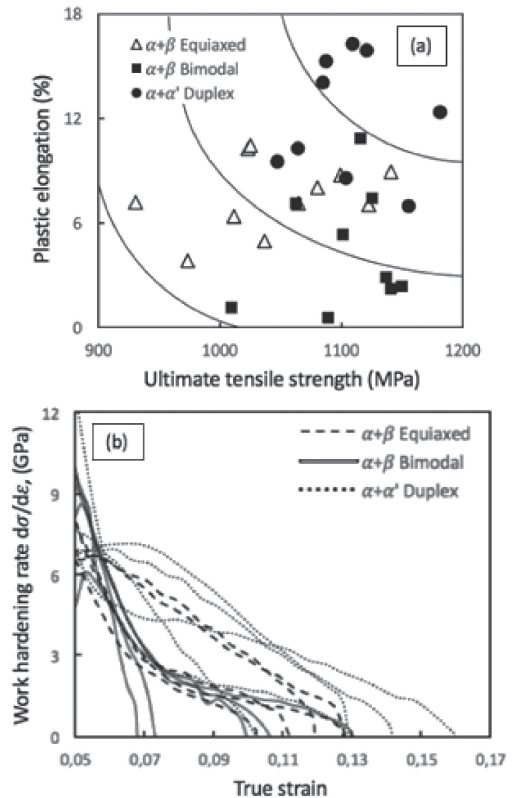


Fig. 3 (a) Plastic elongation ultimate tensile stress (UTS) balance for different microstructures and (b) dynamic work hardening rate evolution for different microstructures of  $\alpha + \beta$  equiaxed,  $\alpha + \beta$  bimodal and  $\alpha + \alpha'$  in Ti-6Al-2Sn-4Zr-2Mo-Si alloy.

boosting regression tree algorithm allowed the evaluation of the importance of the morphology (the type of microstructure), grain size, and phase proportion for each mechanical property (proof stress, UTS, plastic elongation, and work-hardening).

The lightweight  $\text{Ti}_2\text{AlNb}$  phase (O phase)-based titanium intermetallic alloys are expected to be used for high temperature applications.  $(\text{O} + \text{Ti}_3\text{Al} (\alpha_2))$ -type Ti-27.5Al-13Nb was recently developed by Tang *et al.* [69]; however, its ductility was limited at room temperature, in particular, when its microstructure was fully lamellar. Subsequently, its ductility was improved through grain refinement by adding a small amount of boron (B) and heat treatment to produce a duplex microstructure composed of a globular  $\alpha_2$  phase and an  $(\text{O} + \alpha_2)$  lamellar structure. In addition to ductility, the fatigue properties are also important for this type of alloy for applications in automobile and aircraft parts.

Hagiwara and Kitashima [70] examined the high-cycle fatigue (HCF) and very high-cycle fatigue (VHCF) properties of B-free and 0.1 mass% B-modified Ti-27.5Al-13Nb alloy at room temperature. HCF tests were performed in tension-tension mode at an R ratio of 0.1 and a frequency of 10 Hz, while VHCF tests were performed using an ultrasonic resonance fatigue test machine at an R ratio of  $-1$  and a frequency of 20 kHz. With the addition of 0.1 mass% B, the prior  $\text{B}_2$  (Cs-Cl type structure) grain size of an ingot reduced significantly, from  $600\text{--}1000 \mu\text{m}$  for the B-free alloy to  $100\text{--}250 \mu\text{m}$ . The 0.1 mass% B-modified Ti-27.5Al-13Nb alloy with a duplex microstructure consisting of a globular  $\alpha_2$

phase and a lamellar microstructure exhibits superior elongation of 6.1% at room temperature. The HCF curve of the 0.1 mass% B-modified Ti-27.5Al-13Nb alloy with a duplex microstructure is almost the same as that of a Ti-6Al-4V alloy with a fully lamellar microstructure. Despite the prolonged fatigue life in the HCF of the 0.1 mass% B-modified Ti-27.5Al-13Nb and Ti-6Al-4V alloys, the fatigue life in the VHCF region was not improved in these alloys by the addition of 0.1 mass% B.

## 5. Biomedical Applications

Niobium (Nb), which is a  $\beta$ -stabilizing element, exhibits low cytotoxicity and is widely used in  $\beta$ -type titanium alloys [71]. Furthermore, Nb is a  $\beta$ -isomorphous-type element; thus, it does not form intermetallic compounds with Ti. In addition, O is generally an impurity element in titanium; however, optimize the use of O improves the mechanical properties owing to solid-solution strengthening in Ti and is advantageous from the view point of cost reduction of Ti.

Ueda *et al.* [72] investigated the effect of Nb and O contents on the microstructure and mechanical properties of Ti-(5–25)Nb-(0.5–1)O alloys to develop ( $\alpha + \beta$ )-type Ti-Nb-O alloys for biomedical applications. The formation of  $\alpha'$ -martensite was observed in the Ti-5Nb-yO ( $y = 0.5–1$  mass%) alloys after quenching. An increase in the Nb content to 10 mass% leads to the formation of  $\alpha'$ - and  $\alpha''$ -martensite. Further increases in the Nb content to 15 and 20 mass% leads to the formation of  $\alpha''$ -martensite. The addition of oxygen increased the distribution coefficient of Nb and accelerated the distribution of Nb in the  $\beta$ -phase, which in turn led to an increase in the boundary temperature for the formation of  $\alpha'$ - and  $\alpha''$ -martensite in the Ti-10Nb-yO alloys. The Ti-5Nb-(0.5–0.75)O alloys exhibited greater elongation than that of the Ti-6Al-4V ELI alloy. The Ti-5Nb-(0.5–0.75)O alloys exhibited an elastic modulus of 95 GPa, which is lower than that of the Ti-6Al-4V ELI alloy. Ion elution from the Ti-5Nb-(0.5–0.75)O alloys into 0.1 M NaCl-0.1 M lactic acid solution is similar to that from the Ti-6Al-4V ELI alloy. Therefore, the corrosion resistance of the Ti-5Nb-0.5O and Ti-5Nb-0.75O alloys in simulated body fluid were similar to that of the Ti-6Al-4V ELI alloy. Furthermore, the Ti-5Nb-0.5O alloy did not exhibit cytotoxicity against fibroblasts from the lung of Chinese hamsters (V79 cells), indicating that its excellent biocompatibility. Finally, they have proposed Ti-5Nb-(0.5–0.75)O alloys for low-cost type titanium alloys for biomedical applications because these alloys exhibit an excellent balance of strength and ductility, as well as a lower elastic modulus and similar biocompatibility to that of Ti-6Al-4V ELI alloy.

Corrosion of metallic implant devices is not a direct cause of fracture, but leads to toxicity, such as metal allergies. Therefore, when metallic materials are used in medical devices, it is important to investigate their corrosion behavior to ensure biosafety. Ti alloys occasionally come in contact with other metals *in vivo*. For example, in artificial hip joints, a combination of Ti-6Al-4V and Co-Cr-Mo alloys is employed to form the stem and head, respectively. The Ti-6Al-4V alloy exhibits excellent corrosion resistance in the human body when used alone. However, even in the case of

Ti-6Al-4V alloy, there is a possibility for galvanic corrosion to take place when it is used contacting with other metals.

The galvanic corrosion behavior of Ti-6Al-4V ELI alloy for biomedical applications was compared with those of Co-Cr-Mo alloy, 316L-type stainless steel, and Zr-1Mo alloy for biomedical applications by Manaka *et al.* [73]. They prepared coupled specimens of Ti-6Al-4V alloy, Co-Cr-Mo alloy, 316L-type stainless steel or Zr-1Mo alloy for galvanic corrosion tests in saline. The coupling of the Ti-6Al-4V ELI and Co-Cr-Mo alloys did not exhibit localized corrosion and maintained highly stable passive films. When the 316L-type stainless steel and Co-Cr-Mo alloy were coupled, temporary localized corrosion occurred. Similarly, in the coupling of Zr-1Mo and Co-Cr-Mo alloys, temporary localized corrosion occurred. However, both 316L type stainless steel and Zr-1Mo alloy repassivated spontaneously with immersion time. The degree of localized corrosion of the Zr-1Mo alloy was smaller than that of the 316L-type stainless steel. No galvanic current was observed when the Ti-6Al-4V ELI and Co-Cr-Mo alloys were coupled. A slight galvanic current flowed when the 316L-type stainless steel or the Zr-1Mo alloy was coupled with the other alloys. However, the galvanic current with the Zr-1Mo alloy coupling recovered to zero after a certain period owing to re-passivation. No metal ions were detected in the couplings with Zr-1Mo.

Implant surfaces are, in general, roughened to achieve rapid and strong osseointegration, but surface roughening increases the risk of bacterial attachment and growth [74]. Antibacterial surface modification is required to solve this problem; however, it would exhibit toxicity, which reduces biocompatibility. Therefore, surface modification processes with antibacterial properties and improved bone compatibility are necessary. In this case, controlling the bactericidal activity is important [75]. TiO<sub>2</sub> surface modifications offer better controllability of the antibacterial effect because their bactericidal effect is only active when exposed to light compared to other antibacterial surface modifications. Additionally, the photocatalytic decomposition of hydrocarbon contaminations and photoinduced hydrophilic reactions improve cell attachment and calcification [76]. Therefore, photocatalytic TiO<sub>2</sub> coatings can exhibit controllable antibacterial properties and high bone compatibility. Previously, Au-added TiO<sub>2</sub> layers formed by the thermal oxidation of Ti-(4–10) mol% Au alloys for dental implants were reported to exhibit photoinduced organic decomposition [77] and antibacterial properties [78] under visible-light irradiation. However, this process cannot be applied to implant bodies directly because commercially available Ti dental implants usually do not contain Au.

Ueda *et al.* [79] successfully fabricated visible-light-photo catalytically active TiO<sub>2</sub> layers on commercially pure Ti (CP Ti) substrates by Au sputtering and thermal oxidation to prevent infection in dental implants, and then investigated their antibacterial properties. Pure Au and Ti-(60, 40) mol% Au alloy films with thicknesses of 10~47 nm were sputtered onto CP Ti, followed by thermal oxidation in air at 873 K (600°C) for 1.8 ks to form TiO<sub>2</sub> layers. The antibacterial properties of Au-added TiO<sub>2</sub> layers substrate against *Escherichia coli*, cytotoxicity, and bonding strength were evaluated. The highest antibacterial activity under

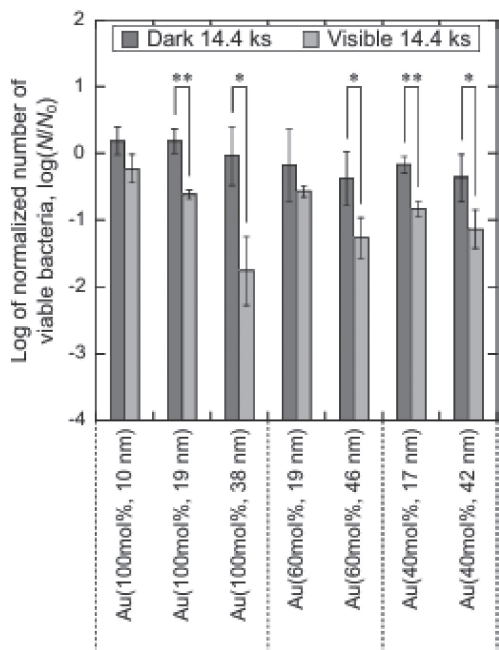


Fig. 4 Log of normalized number of viable bacteria on the TiO<sub>2</sub> layers formed on Ti with Au-Ti sputtered films after placement in the dark and irradiation with visible light under the irradiating conditions of irradiating intensity ( $I$ ) = 1 mW·cm<sup>-2</sup> and irradiation time ( $t_{\text{vis}}$ ) = 14.4 ks. Error bars correspond to one standard deviation. \* and \*\*: significant difference of  $P < 0.05$  and  $0.01$ , respectively.

visible-light irradiation was obtained when the sputtered film was pure Au with a thickness of 38 nm as shown in Fig. 4 [79]. Compared with as-polished CP Ti, the number of viable mouse osteoblast-like cells and human gingival fibroblasts on Au-added TiO<sub>2</sub> layers increased after placement in the dark, but decreased after visible-light irradiation. The best balance of the antibacterial property and bonding strength was achieved in the Ti-40 mol%Au sputtered film with a thickness of 42 nm.

Low Young's modulus titanium alloys such as the  $\beta$ -type Ti-29Nb-13Ta-4.6Zr alloy (TNTZ) [33] are suitable for use as spinal fixation rods because their flexibility is expected to reduce adjacent intervertebral disorder. Simultaneously, the spinal fixation rod requires high strength to prevent secondary fracture [80]. The  $\beta$ -type titanium alloy exhibits the lowest Young's modulus in the single  $\beta$ -phase obtained by rapid cooling from the solution treatment over the  $\beta$ -transus temperature, while the strength increases with aging treatment after solution treatment owing to the  $\alpha$ -phase precipitation; however, the Young's modulus increases with aging treatment.

Based on this characteristic of  $\beta$ -type titanium alloys, Nakai *et al.* [81] have proposed a concept to satisfy the above-mentioned requirement for spinal fixation rods, in which the rod to fix the lower side of the lumbar vertebrae, which is most likely to be broken, is aged for precipitation strengthening to achieve high strength, whereas the rod to fix the upper side of the lumbar vertebrae is solution-treated to achieve a low Young's modulus and flexibility. The effectiveness of this concept was evaluated by comparing two types of rods using a finite element analysis. Namely, one type of rod had a high Young's modulus (110 GPa)

throughout, while the other type had a lower Young's modulus (60 GPa) at the lower part of the rod (S1-L3 of the lumbar vertebrae) and a high Young's modulus (110 GPa) at the upper part of the rod (L3-L2 of the lumbar vertebrae), and the latter was a rod with a partially lowered Young's modulus. Finite element analysis proved that a rod with a partially lowered Young's modulus (60 GPa) can simultaneously enhance both flexibility and fixity compared with a rod with a high Young's modulus (110 GPa) throughout.

To fabricate the partially lowered Young's modulus rod, the rod subjected to the aging treatment was partially heated to over the  $\beta$ -transus temperature in a rapid manner leading to a partially solution-treatment by applying high-frequency induction heating (IH-treatment) followed by rapid cooling (water quenching) without maintaining the heated condition. In a TNTZ rod, a high Young's modulus of approximately 110 GPa can be obtained by aging treatment, whereas a low Young's modulus of approximately 60 GPa can be obtained by solution-treatment [82].

## 6. Recycling

Owing to the increasing demand for titanium products, a large amount of titanium scrap and its alloys will be generated. As titanium smelting process consumes high energy and generates a large amount of carbon dioxide (CO<sub>2</sub>), recycling titanium scrap is important from the perspectives of economic rationality and environmental impact. The recycling of titanium scrap tends to increase the oxygen concentration. Therefore, an upgraded recycling process is required to convert titanium scrap with high oxygen concentration into titanium with low oxygen concentration.

Various methods have been developed to remove oxygen from Ti [83]. Many of them utilize thermochemical reactions with metal deoxidants or electrochemical reactions in molten salt fluxes. However, Ouchi *et al.* [84] reported a new deoxidation technique for Ti using the vapor of rare earth metals with high vapor pressures, such as samarium (Sm), europium (Eu), thulium (Tm), and ytterbium (Yb). It was confirmed that Eu did not decrease the oxygen concentration in the Ti samples below 1,000 mass ppm. However, the Sm, Tm, and Yb vapors decreased the oxygen concentration in the Ti samples through their oxide formation reactions as shown in Fig. 5 [84]. The Tm vapor can deoxidize Ti at or below the oxygen concentration of the Ti sponge produced by the Kroll process (500 mass ppm O).

## 7. Summary

This study reviews articles on recent research and development of titanium alloys, especially the AM of titanium alloys. The AM of titanium alloys is expected to continue to be developed further in the future. However, the research and development history of titanium alloys is shorter than that of other major practical metallic materials. In particular, the history of their manufacturing technologies, microstructures, and properties are yet to be studied. The research and development of titanium alloys is an ongoing progress.

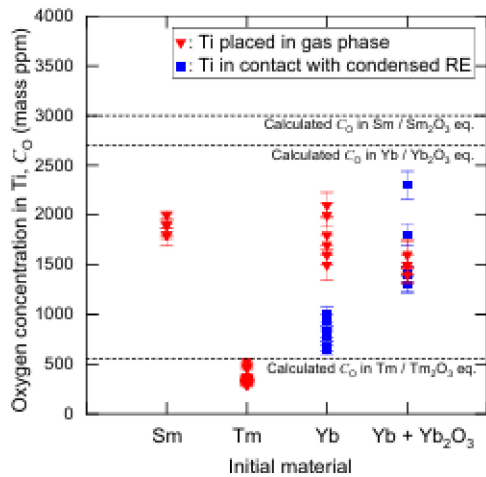


Fig. 5 Comparisons of the analyzed and calculated oxygen concentrations in the Ti samples with an initial oxygen concentration of 3,600~4,300 ppm after the deoxidation experiments utilizing Sm, Tm and Yb metals, and Yb metal with  $\text{Yb}_2\text{O}_3$  at 1300 K (1,027°C). The error bars show the analyzed error of the oxygen concentrations in the Ti samples.

## REFERENCES

- [1] Special Issue on Research and Developments in Titanium and Its Alloys, *Mater. Trans.* **45** (2004) 1539–1664.
- [2] Special Issue on Low Cost Reduction Processes, Roles of Low Cost Elements and Interstitial Elements, and Microstructural Control for Generalization of Titanium Alloys, *Mater. Trans.* **50** (2009) 2703–2771.
- [3] Special Issue on Recent Advances in Research and Development of Titanium and Its Alloys, *Mater. Trans.* **54** (2013) 127–175.
- [4] Special Issue on New Proposals on Titanium Production and Molten Salts, *Mater. Trans.* **58** (2017) 305–394.
- [5] Special Issue on Latest Research and Development of Structural and Functional Titanium-Based Materials, *Mater. Trans.* **60** (2019) 1732–1872.
- [6] <https://jitit.smoosy.atlas.jp/ja>.
- [7] M. Niinomi, M. Ikeda, T. Narushima, T. Nakano and H. Hosoda (eds.), *Fundamental and Applications of Titanium*, (Uchida Rokakuho, Tokyo, 2023).
- [8] Research and Development in the Processing, Microstructure, and Properties of Titanium and Its Alloy, *Mater. Trans.* **64** (2023) 1–164.
- [9] S.-H. Sun, K. Hagihara, T. Ishimoto, R. Suganuma, Y.-F. Xue and T. Nakano: Comparison of microstructure, crystallographic texture, and mechanical properties in Ti–15Mo–5Zr–3Al alloys fabricated via electron and laser beam powder bed fusion technologies, *Addit. Manuf.* **47** (2021) 102329.
- [10] T.J. Bruno and P.D.N. Svoronos: *CRC Handbook of Basic Tables for Chemical Analysis: Data-Driven Methods and Interpretation*, 4th ed., (CRC Press, Florida, 2020).
- [11] H. Amano, T. Ishimoto and T. Nakano: Review—Importance of Atmospheric Gas Selection in Metal Additive Manufacturing: Effects on Spatter, Microstructure, and Mechanical Properties, *Mater. Trans.* **64** (2023) 2–9.
- [12] T. Ishimoto and T. Nakano: Review — Microstructural Control and Functional Enhancement of Light Metal Materials via Metal Additive Manufacturing, *Mater. Trans.* **64** (2023) 10–16.
- [13] S.-H. Lee, M. Todai, M. Tane, K. Hagihara, H. Nakajima and T. Nakano: Biocompatible low Young's modulus achieved by strong crystallographic elastic anisotropy in Ti–15Mo–5Zr–3Al alloy single crystal, *J. Mech. Behav. Biomed. Mater.* **14** (2012) 48–54.
- [14] S. Ziegelmeier, P. Christou, F. Wöllecke, C. Tuck, R. Goodridge, R. Hague, E. Krampe and E. Wintermantel: An experimental study into the effects of bulk and flow behaviour of laser sintering polymer powders on resulting part properties, *J. Mater. Process. Technol.* **215** (2015) 239–250.
- [15] M. Okugawa, Y. Isono, Y. Koizumi and T. Nakano: Raking Process for Powder Bed Fusion of Ti–6Al–4V Alloy Powder Analyzed by Discrete Element Method, *Mater. Trans.* **64** (2023) 37–43.
- [16] S. Das: Physical Aspects of Process Control in Selective Laser Sintering of Metals, *Adv. Eng. Mater.* **5** (2003) 701–711.
- [17] M. Nakamoto and T. Tanaka: Evaluation of Liquid/Solid Interfacial Property for Ti–6 mass%Al–4 mass%V Alloy Using Electron-Beam Additive Manufacturing, *Mater. Trans.* **64** (2023) 50–53.
- [18] P. Edwards and M. Ramulu: Fatigue performance evaluation of selective laser melted Ti–6Al–4V, *Mater. Sci. Eng. A* **598** (2014) 327–337.
- [19] A. Takase: Residual Stress and Phase Stability of Titanium Alloys Fabricated by Laser and Electron Beam Powder Bed Fusion Techniques, *Mater. Trans.* **64** (2023) 17–24.
- [20] K. Shimagami, T. Ito, Y. Toda, A. Yumoto and Y. Yamabe-Mitarai: Effects of Zr and Si addition on high-temperature mechanical properties and microstructure in Ti–10Al–2Nb-based alloys, *Mater. Sci. Eng. A* **756** (2019) 46–53.
- [21] T. Kuroda, H. Masuyama, Y. Toda, T. Matsunaga, T. Ito, M. Watanabe, R. Ozasa, T. Ishimoto, T. Nakano, M. Shimojo and Y. Yamabe-Mitarai: Microstructure Evolution and High-Temperature Mechanical Properties of Ti–6Al–4Nb–4Zr Fabricated by Selective Laser Melting, *Mater. Trans.* **64** (2023) 95–103.
- [22] T. Kuzumaki, O. Ujiie, H. Ichinose and K. Ito: Mechanical Characteristics and Preparation of Carbon Nanotube Fiber-Reinforced Ti Composite, *Adv. Eng. Mater.* **2** (2000) 416–418.
- [23] Z.-Y. Hu, Z.-H. Zhang, X.-W. Cheng, F.-C. Wang, Y.-F. Zhang and S.-L. Li: A review of multi-physical fields induced phenomena and effects in spark plasma sintering: Fundamentals and applications, *Mater. Des.* **191** (2020) 108662.
- [24] S. Mohammad Bagheri, M. Vajdi, F. Sadegh Moghanlou, M. Sakkaki, M. Mohammadi, M. Shokouhimehr and M. Shahedi Asl: Numerical modeling of heat transfer during spark plasma sintering of titanium carbide, *Ceram. Int.* **46** (2020) 7615–7624.
- [25] B. Cheng, S. Shrestha and K. Chou: Stress and deformation evaluations of scanning strategy effect in selective laser melting, *Addit. Manuf.* **12** (2016) 240–251.
- [26] M. Dong, W. Zhou, Z. Zhou and N. Nomura: Microstructures and Mechanical Properties of Carbon-Added Ti Composites Fabricated by Laser Powder Bed Fusion or Spark Plasma Sintering, *Mater. Trans.* **64** (2023) 54–60.
- [27] K. Cho, N. Morita, H. Matsuoka, H.Y. Yasuda, M. Todai, M. Ueda, M. Takeyama and T. Nakano: Influence of Input Energy Density on Morphology of Unique Layered Microstructure of  $\gamma$ -TiAl Alloys Fabricated by Electron Beam Powder Bed Fusion, *Mater. Trans.* **64** (2023) 44–49.
- [28] M. Todai, T. Nakano, T. Liu, H.Y. Yasuda, K. Hagihara, K. Cho, M. Ueda and M. Takeyama: Effect of building direction on the microstructure and tensile properties of Ti–48Al–2Cr–2Nb alloy additively manufactured by electron beam melting, *Addit. Manuf.* **13** (2017) 61–70.
- [29] K. Cho, R. Kobayashi, J.Y. Oh, H.Y. Yasuda, M. Todai, T. Nakano, A. Ikeda, M. Ueda and M. Takeyama: Influence of unique layered microstructure on fatigue properties of Ti–48Al–2Cr–2Nb alloys fabricated by electron beam melting, *Intermetallics* **95** (2018) 1–10.
- [30] K. Cho, N. Morita, H. Matsuoka, H.Y. Yasuda, M. Todai, M. Ueda, M. Takeyama and T. Nakano: Influence of Input Energy Density on Morphology of Unique Layered Microstructure of  $\gamma$ -TiAl Alloys Fabricated by Electron Beam Powder Bed Fusion, *Mater. Trans.* **64** (2023) 44–49.
- [31] K. Gokan, Y. Yamagishi, K. Mizuta and K. Kakehi: Effect of Process Parameters on the Microstructure and High-Temperature Strengths of Titanium Aluminide Alloy Fabricated by Electron Beam Melting, *Mater. Trans.* **64** (2023) 104–110.
- [32] A. Matsugaki, T. Matsuzaka and T. Nakano: Review—Metal Additive Manufacturing of Titanium Alloys for Control of Hard Tissue Compatibility, *Mater. Trans.* **64** (2023) 25–30.
- [33] M. Niinomi, T. Hattori, K. Morikawa, T. Kasuga, A. Suzuki, H. Fukui and S. Niwa: Development of Low Rigidity  $\beta$ -type Titanium Alloy for Biomedical Applications, *Mater. Trans.* **43** (2002) 2970–2977.
- [34] T. Ishimoto, K. Hagihara, K. Hisamoto, S.-H. Sun and T. Nakano: Crystallographic texture control of beta-type Ti–15Mo–5Zr–3Al alloy by selective laser melting for the development of novel implants with a

- biocompatible low Young's modulus, *Scr. Mater.* **132** (2017) 34–38.
- [35] N. Ikeo, T. Matsumi, T. Ishimoto, R. Ozasa, A. Matsugaki, T. Matsuzaka, O. Gokcekaya, Y. Takigawa and T. Nakano: Fabrication of Ti-Alloy Powder/Solid Composite with Uniaxial Anisotropy by Introducing Unidirectional Honeycomb Structure via Electron Beam Powder Bed Fusion, *Crystals* **11** (2021) 1074.
- [36] S. Ponader, E. Vairaktaris, P. Heintl, C. Wilmowsky, A. Rottmair, C. Körner, R.F. Singer, S. Holst, K.A. Schlegel, F.W. Neukam and E. Nkenke: Effects of topographical surface modifications of electron beam melted Ti–6Al–4V titanium on human fetal osteoblasts, *J. Biomed. Mater. Res. A* **84A** (2008) 1111–1119.
- [37] N.W. Hrabec, P. Heintl, R.K. Bordia, C. Körner and R.J. Fernandes: Maintenance of a bone collagen phenotype by osteoblast-like cells in 3D periodic porous titanium (Ti–6Al–4V) structures fabricated by selective electron beam melting, *Connect Tissue Res.* **54** (2013) 351–360.
- [38] C.M. Haslauer, J.C. Springer, O.L.A. Harrysson, E.G. Lobo, N.A. Monteiro-Riviere and D.J. Marcellin-Little: *In vitro* biocompatibility of titanium alloy discs made using direct metal fabrication, *Med. Eng. Phys.* **32** (2010) 645–652.
- [39] N. Ikeo, T. Matsumi, T. Ishimoto, R. Ozasa, A. Matsugaki, T. Matsuzaka, O. Gokcekaya, Y. Takigawa and T. Nakano: Fabrication of Ti-Alloy Powder/Solid Composite with Uniaxial Anisotropy by Introducing Unidirectional Honeycomb Structure via Electron Beam Powder Bed Fusion, *Crystals* **11** (2021) 1074.
- [40] T. Nakano, K. Kaibara, T. Ishimoto, Y. Tabata and Y. Umakoshi: Biological apatite (BAp) crystallographic orientation and texture as a new index for assessing the microstructure and function of bone regenerated by tissue engineering, *Bone* **51** (2012) 741–747.
- [41] A. Matsugaki, F. Nakamura, R. Takehana, T. Todo, R. Fukushima, T. Matsuzaka, R. Ozasa, T. Ishimoto, S. Miyabe and T. Nakano: Control of Stem Cell Fate and Function by Engineered Surface Topography Using Metal Additive Manufacturing Technology, *J. Smart Process.* **10** (2021) 261–264.
- [42] A. Matsugaki, T. Matsuzaka, A. Murakami, P. Wang and T. Nakano: 3D Printing of Anisotropic Bone-Mimetic Structure with Controlled Fluid Flow Stimuli for Osteocytes: Flow Orientation Determines the Elongation of Dendrites, *Int. J. Bioprint.* **6** (2020) 293.
- [43] M. Todai, T. Nagase, T. Hori, A. Matsugaki, A. Sekita and T. Nakano: Novel TiNbTaZrMo high-entropy alloys for metallic biomaterials, *Scr. Mater.* **129** (2017) 65–68.
- [44] T. Nagase, M. Todai and T. Nakano: Development of Ti–Zr–Hf–Y–La high-entropy alloys with dual hexagonal-close-packed structure, *Scr. Mater.* **186** (2020) 242–246.
- [45] T. Nagase, Y. Iijima, A. Matsugaki, K. Ameyama and T. Nakano: Design and fabrication of Ti–Zr–Hf–Cr–Mo and Ti–Zr–Hf–Co–Cr–Mo high-entropy alloys as metallic biomaterials, *Mater. Sci. Eng. C* **107** (2020) 110322.
- [46] Y. Iijima, T. Nagase, A. Matsugaki, P. Wang, K. Ameyama and T. Nakano: Design and development of Ti–Zr–Hf–Nb–Ta–Mo high-entropy alloys for metallic biomaterials, *Mater. Des.* **202** (2021) 109548.
- [47] R. Ozasa, A. Matsugaki, T. Ishimoto and T. Nakano: Review — Research and Development of Titanium-Containing Biomedical High Entropy Alloys (BioHEAs) Utilizing Rapid Solidification via Laser-Powder Bed Fusion, *Mater. Trans.* **64** (2023) 31–36.
- [48] T. Hori, T. Nagase, M. Todai, A. Matsugaki and T. Nakano: Development of non-equiatomic Ti-Nb-Ta-Zr-Mo high-entropy alloys for metallic biomaterials, *Scr. Mater.* **172** (2019) 83–87.
- [49] T. Ishimoto, R. Ozasa, K. Nakano, M. Weinmann, C. Schnitter, M. Stenzel, A. Matsugaki, T. Nagase, T. Matsuzaka, M. Todai, H.S. Kim and T. Nakano: Development of TiNbTaZrMo bio-high entropy alloy (BioHEA) super-solid solution by selective laser melting, and its improved mechanical property and biocompatibility, *Scr. Mater.* **194** (2021) 113658.
- [50] Q. Jia, P. Rometsch, P. Kürsteiner, Q. Chao, A. Huang, M. Weyland, L. Bourgeois and X. Wu: Selective laser melting of a high strength Al-Mn-Sc alloy: Alloy design and strengthening mechanisms, *Acta Mater.* **171** (2019) 108–118.
- [51] F.H. Froes, C.F. Yolton, J.M. Capenos, M.G.H. Wells and J.C. Williams: The Relationship between Microstructure and Age Hardening Response in the Metastable Beta Titanium Alloy Ti-11.5 Mo-6 Zr-4.5 Sn (beta III), *Metall. Mater. Trans. A* **11** (1980) 21–31.
- [52] M. Niinomi, M. Nakai, M. Hendrickson, P. Nandwana, T. Alam, D. Choudhuri and R. Banerjee: Influence of oxygen on omega phase stability in the Ti-29Nb-13Ta-4.6Zr alloy, *Scr. Mater.* **123** (2016) 144–148.
- [53] K. Chou and E.A. Marquis: Oxygen effects on  $\omega$  and  $\alpha$  phase transformations in a metastable  $\beta$  Ti–Nb alloy, *Acta Mater.* **181** (2019) 367–376.
- [54] S. Kobayashi and S. Okano: Acceleration of Isothermal  $\omega$  Phase Formation by Oxygen Addition in Ti–Nb Alloys during Cooling Process, *Mater. Trans.* **64** (2023) 71–77.
- [55] T. Inamura, Y. Fukui, H. Hosoda, K. Wakashima and S. Miyazaki: Relationship between Texture and Macroscopic Transformation Strain in Severely Cold-Rolled Ti-Nb-Al Superelastic Alloy, *Mater. Trans.* **45** (2004) 1083–1089.
- [56] S. Kawano, S. Kobayashi and S. Okano: Effect of Oxygen Addition on the Formation of  $\alpha''$  Martensite and Athermal  $\omega$  in Ti–Nb Alloys, *Mater. Trans.* **60** (2019) 1842–1849.
- [57] T. Ozaki, H. Matsumoto, S. Watanabe and S. Hanada: Beta Ti Alloys with Low Young's Modulus, *Mater. Trans.* **45** (2004) 2776–2779.
- [58] Y. Mantani and Y. Takemoto: Structural Changes due to Heating and Stress Loading of Metastable Quenched Martensite Structures in Ti–(10–20)mass% Nb Alloys, *Mater. Trans.* **64** (2023) 78–85.
- [59] H. Matsumoto and H. Ito: High Temperature Tensile Deformation Mode and Microstructural Conversion of Ti–6Al–4V Alloy with the ( $\alpha + \alpha'$ ) Duplex Starting Microstructure, *Mater. Trans.* **60** (2019) 1833–1841.
- [60] E. Hall: The Deformation and Ageing of Mild Steel: III Discussion of Results, *Proc. Phys. Soc. London, Sect. B* **64** (1951) 747–753.
- [61] S. Miyazaki, K. Shibata and H. Fujita: Effect of specimen thickness on mechanical properties of polycrystalline aggregates with various grain sizes, *Acta Metall.* **27** (1979) 855–862.
- [62] T. Fukumaru, H. Hidaka, T. Tsuchiyama and S. Takaki: Effect of Wire Diameter and Grain Size on Tensile Properties of Austenitic Stainless Steel Wire, *Tetsu-to-Hagané* **91** (2005) 828–833.
- [63] H. Takebe, K. Mori, K. Takahashi and H. Fujii: Effects of Thickness and Grain Size on Tensile Properties of Pure Titanium Thin Gauge Sheets, *Proc. 13th World Conf. on Titanium*, (2015) pp. 491–494.
- [64] H. Takebe and K. Ushioda: Effects of Grain Size, Thickness and Tensile Direction on Yield Behavior of Pure Titanium Sheet, *Mater. Trans.* **64** (2023) 86–94.
- [65] R.R. Boyer: An overview on the use of titanium in the aerospace industry, *Mater. Sci. Eng. A* **213** (1996) 103–114.
- [66] O. Dumas, L. Malet, B. Hary, F. Prima and S. Godet: Crystallography and reorientation mechanism upon deformation in the martensite of an  $\alpha$ - $\alpha'$  Ti-6Al-4V dual-phase microstructure exhibiting high work-hardening rate, *Acta Mater.* **205** (2021) 116530.
- [67] H. Matsumoto, H. Yoneda, K. Sato, S. Kurosu, E. Maire, D. Fabregue, T.J. Konno and A. Chiba: Room-temperature ductility of Ti–6Al–4V alloy with  $\alpha'$  martensite microstructure, *Mater. Sci. Eng. A* **528** (2011) 1512–1520.
- [68] I. Séchépée, P. Paulain, Y. Nagasaki, R. Tanaka, H. Matsumoto and V. Velay: Excellent Balance of Ultimate Tensile Strength and Ductility in a Ti–6Al–2Sn–4Zr–2Mo–Si Alloy Having Duplex  $\alpha + \alpha'$  Microstructure: Effect of Microstructural Factors from Experimental Study and Machine Learning, *Mater. Trans.* **64** (2023) 111–120.
- [69] F. Tang and M. Hagiwara: Tensile properties and creep behavior of a new Ti-Al-Nb intermetallic alloy with an O+ $\alpha_2$  microstructure, *Metall. Mater. Trans. A* **34** (2003) 633–643.
- [70] M. Hagiwara and T. Kitashima: High Cycle Fatigue and Very High Cycle Fatigue of Orthorhombic (O +  $\alpha_2$ )-Type Ti–27.5Nb–13Al Alloy with and without B and Fatigue Striation Analysis in Comparison with ( $\alpha + \beta$ )-Type Titanium Alloys, *Mater. Trans.* **64** (2023) 121–130.
- [71] D. Kuroda, M. Niinomi, M. Morinaga, Y. Kato and T. Yashiro: Design and mechanical properties of new  $\beta$  type titanium alloys for implant materials, *Mater. Sci. Eng. A* **243** (1998) 244–249.
- [72] K. Ueda, M. Omiya, K. Kato, H. Kanetaka and T. Narushima: Effect of Niobium and Oxygen Contents on Microstructure and Mechanical Properties of  $\alpha + \beta$ -Type Ti–(5–25)Nb–(0.5–1)O (mass%) Alloys for Biomedical Applications, *Mater. Trans.* **64** (2023) 138–146.
- [73] T. Manaka, Y. Tsutsumi, Y. Takada, P. Chen, M. Ashida, K. Doi, H. Katayama and T. Hanawa: Galvanic Corrosion among Ti–6Al–4V ELI

- Alloy, Co–Cr–Mo Alloy, 316L-Type Stainless Steel, and Zr–1Mo Alloy for Orthopedic Implants, *Mater. Trans.* **64** (2023) 131–137.
- [74] A. Mombelli: Microbiology and antimicrobial therapy of peri-implantitis, *Periodontol.* **2000** **28** (2002) 177–189.
- [75] J. Wu, K. Ueda and T. Narushima: Fabrication of Ag and Ta co-doped amorphous calcium phosphate coating films by radiofrequency magnetron sputtering and their antibacterial activity, *Mater. Sci. Eng. C* **109** (2020) 110599.
- [76] H. Aita, N. Hori, M. Takeuchi, T. Suzuki, M. Yamada, M. Anpo and T. Ogawa: The effect of ultraviolet functionalization of titanium on integration with bone, *Biomaterials* **30** (2009) 1015–1025.
- [77] T. Ueda, S. Sado, K. Ueda and T. Narushima: TiO<sub>2</sub> layers on Ti–Au alloy formed by two-step thermal oxidation and their photocatalytic activity in visible-light, *Mater. Lett.* **185** (2016) 290–294.
- [78] T. Ueda, K. Ueda, K. Ito, K. Ogasawara, H. Kanetaka, T. Mokudai, Y. Niwano and T. Narushima: Visible-light-responsive antibacterial activity of Au-incorporated TiO<sub>2</sub> layers formed on Ti–(0–10)at%Au alloys by air oxidation, *J. Biomed. Mater. Res. A* **107** (2019) 991–1000.
- [79] T. Ueda, R. Koizumi, K. Ueda, K. Ito, K. Ogasawara, H. Kanetaka and T. Narushima: Antibacterial Properties of TiO<sub>2</sub> Layers Formed by Au-Sputtering and Thermal Oxidation of Titanium under Visible Light, *Mater. Trans.* **64** (2023) 155–164.
- [80] R. Lafage, B.G. Line, S. Gupta, B. Liabaud, F. Schwab, J.S. Smith, J.L. Gum, C.P. Ames, R. Hostin, G.M. Mundis, Jr., H.J. Kim, S. Bess, E. Klineberg and V. Lafage: Orientation of the Upper-most Instrumented Segment Influences Proximal Junctional Disease Following Adult Spinal Deformity Surgery, *Spine* **42** (2017) 1570–1577.
- [81] M. Nakai, K. Narita, K. Kobayashi, K. Sasagawa, M. Niinomi and K. Hasegawa: Concept and Fabrication of Beta-Type Titanium Alloy Rod with Parts Possessing Different Young’s Moduli for Spinal Fixation, *Mater. Trans.* **64** (2023) 147–154.
- [82] M. Nakai, M. Niinomi, T. Akahori, H. Tsutsumi and M. Ogawa: Effect of Oxygen Content on Microstructure and Mechanical Properties of Biomedical Ti–29Nb–13Ta–4.6Zr Alloy under Solutionized and Aged Conditions, *Mater. Trans.* **50** (2009) 2716–2720.
- [83] O. Takeda and T.H. Okabe: Current Status of Titanium Recycling and Related Technologies, *JOM* **71** (2019) 1981–1990.
- [84] T. Ouchi, K. Akaishi, G. Kamimura and T.H. Okabe: Direct Oxygen Removal from Titanium by Utilizing Vapor of Rare Earth Metals, *Mater. Trans.* **64** (2023) 61–70.